engineering proceedings

MDPI

Proceeding Paper

Development and Application of Self-Sensing Materials for Structural Health Monitoring of Civil Engineering Infrastructures †

Rosa Penna, Annavirginia Lambiase *, Gerarda Landi, Giuseppe Lovisi and Luciano Feo

Department of Civil Engineering, University of Salerno, 84084 Fisciano, Italy; rpenna@unisa.it (R.P.); gelandi@unisa.it (G.L.); glovisi@unisa.it (G.L.); lfeo@unisa.it (L.F.)

* Correspondence: annlambiase@unisa.it

† Presented at the 7th edition of the International Conference on Advanced Technologies for Humanity (ICATH 2025), Kenitra, Morocco, 9–11 July 2025.

Abstract

This study examines advanced cementitious composites incorporating Multi-Walled Carbon Nanotubes (MWCNTs), combining experimental investigations and analytical modeling for enhanced Structural Health Monitoring (SHM) applications. The experimental phase assessed the electrical properties of specimens with varying MWCNT contents, identifying a percolation zone between 0.05 wt% and 0.5 wt%. A dispersion protocol using ultrasonic agitation and a surfactant ensured the uniform distribution of CNTs. Furthermore, a novel micromechanical model, based on established polymer matrix approaches, was used to predict electrical conductivity behavior, accounting for nanotube geometry, concentration, waviness, and tunneling effects. Model predictions confirmed its effectiveness in analyzing structure–property relationships in CNT-based cementitious materials.

Keywords: carbon nanotube; smart concrete; Structural Health Monitoring; micromechanical model; cement–matrix composites; piezoresistive modeling

check for updates

Academic Editors: Brahim El Bhiri and Ayman S. Mosallam

Published: 14 October 2025

Citation: Penna, R.; Lambiase, A.; Landi, G.; Lovisi, G.; Feo, L. Development and Application of Self-Sensing Materials for Structural Health Monitoring of Civil Engineering Infrastructures. *Eng. Proc.* **2025**, *112*, 16. https://doi.org/10.3390/engproc2025112016

Copyright: © 2025 by the authors. Licensee MDPI, Basel, Switzerland. This article is an open access article distributed under the terms and conditions of the Creative Commons Attribution (CC BY) license (https://creativecommons.org/licenses/by/4.0/).

1. Introduction

Despite its widespread use and essential role in modern construction, cement-based materials is inherently susceptible to durability issues—such as cracking, corrosion, and degradation—that lead to costly maintenance and compromise the long-term performance of infrastructure. To mitigate these problems, Structural Health Monitoring (SHM) systems have been developed to enhance the safety and prolong the service life of concrete structures [1,2].

Traditional SHM devices—such as strain gauges, piezoelectric transducers, and fiber-optic sensors—have been widely utilized [3–5]; however, they often exhibit limited compatibility with cementitious matrices, mechanical fragility, high manufacturing costs, and complex deployment procedures [6–8]. To overcome these limitations, recent advances in materials science—including the incorporation of micro- and nano-fibers—have enabled the development of cement-based composites with enhanced mechanical properties and, in some cases, self-sensing capabilities [9–19]. Through the incorporation of functional nanomaterials—such as carbon nanofibers, nanotubes, and graphene nanoplatelets—these intelligent materials improve both structural performance and sensing functionality via the piezoresistive effect [20]. This means they can detect variations in electrical signals when subjected to mechanical stress, exhibiting changes in electrical conductivity in response

to internal or external stimuli (e.g., temperature, impact, or mechanical loading), thus allowing for real-time, intrinsic Structural Health Monitoring [21].

Accurately predicting the behavior of these multifunctional composites remains a major challenge, particularly due to the difficulties in achieving a uniform dispersion of nanofillers within the cement matrix, which can severely affect both sensing performance and mechanical properties [22–24]. These limitations, along with the complexities involved in their fabrication, highlight the crucial role of micromechanical modeling in capturing the interactions at the microscale and guiding the design of more reliable and efficient smart cement-based materials.

In recent years, several micromechanical models have been developed that account for the two main mechanisms governing the electrical behavior of CNT-based composites: electron hopping and the formation of conductive networks. Early studies by Deng and Zheng [25] and Takeda et al. [26] focused on polymer matrices, primarily modeling the percolation phenomenon while accounting for the orientation and waviness of carbon nanotubes, but without explicitly distinguishing the contribution of electron hopping. In contrast, Seidel and Lagoudas [27] and Feng and Jiang [28] separated these two mechanisms using approaches based on the Mori–Tanaka theory. More recent models, like those by Alamusi and Hu [29], incorporated three-dimensional resistor networks including tunneling effects, whereas García-Macías et al. [30,31] concentrated on cementitious matrices, considering CNTs agglomeration and uneven dispersion to accurately predict piezoresistive properties.

In this context, the present work explores the electrical response of cementitious composites with MWCNTs through both experimental investigations and micromechanical modeling. Experimental tests were carried out at the Materials and Structures Testing Laboratory of the Department of Civil Engineering at the University of Salerno on samples prepared with different MWCNT contents. Nanotube dispersion was achieved through ultrasonic treatment combined with a surfactant. Electrical conductivity was measured using the four-probe DC method to minimize contact resistance effects.

In order to predict the experimental electrical behavior, a micromechanical model developed by the same authors [32] was employed, without accounting for the contributions of electron hopping as well as the effects of agglomeration and segregation of MWCNTs. The model introduces a novel approach to estimate the thickness of the inter-nanotube matrix region, taking into account the phenomenon of electron tunneling, using well-established principles of quantum mechanics.

2. Experimental Investigation

2.1. Material and Mix Design

Cement-based nanocomposites were prepared using ordinary Portland cement (type 42.5R) [33] as binder material, water, an anionic surfactant (Sodium Dodecyl Sulfate) [34], and industrial-grade Multi-Walled Carbon Nanotubes (MWCNTs) [35] as conductive nanofillers. To enhance the dispersion of MWCNTs in water, the surfactant was added at 0.2% by weight of cement while maintaining a constant water-to-cement ratio of 0.4. Seven different mixtures were prepared with MWCNT contents ranging from 0% to 1.5% by weight of cement, hereafter referred to as M0, M0.025, M0.05, M0.075, M0.5, M1.0, and M1.5. The main MWCNT properties are summarized in Table 1.

Table 1. Physico-chemical and geometrical characteristics of MWCNTs [35].

Property	Value
Purity	>90% in weight
Ash content	<1.5% in weight
Length	10–30 μm
Outer mean diameter	10–30 nm
Inner mean diameter	5–10 nm
Specific surface area	>200 m^2/g
Bulk density	0.06 g/cm^3

2.2. Dispersion of MWCNTs

Proper dispersion of CNTs is essential for establishing an effective conductive network, yet it is often hindered by their strong tendency to agglomerate due to hydrophobicity, high aspect ratio, and strong Van der Waals interactions. To address this challenge and achieve good homogeneity, a specific sequence of mixing processes was implemented to ensure effective dispersion of the nanofiller in water before adding it to the cement powder. In particular, two of the most efficient dispersion techniques were employed: the ultrasonication method combined with the use of surfactants.

The suspensions were prepared at the NANO_MATES center (Research Centre for NANOMAterials and NANOTEchnologies) of the University of Salerno. The MWCNTs were mixed in water following the addition of the surfactant (Figure 1a). After an initial 5 min mixing with a mechanical stirrer, dispersions were sonicated at room temperature applying constant energy by an ultrasound tip (UP400S, Hielscher Ultrasonics GmbH, Germany) at the maximum power of ultrasound for 20 min. The sonicator was operated at an amplitude of 100% at 0.5 cycles to prevent overheating of the suspensions (Figure 1b,c).

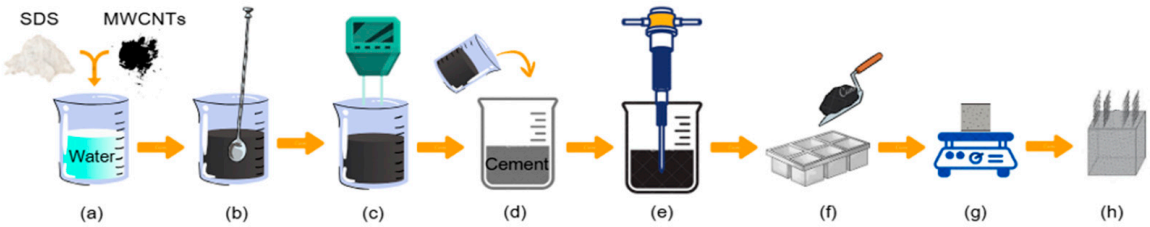


Figure 1. Preparation procedure of cementitious pastes with MWCNTs: (**a**) addition of MWCNTs and surfactant to water; (**b**) mechanical stirring; (**c**) sonication; (**d**) addition of MWCNT suspension to the cement powder; (**e**) mechanical mixing; (**f**) molds casting; (**g**) vibration; (**h**) embedding of copper electrodes.

2.3. Preparation of Specimens

A total of 42 cementitious samples with a cube shape of 50 mm side were prepared to carry out the overall experimental program of this research. Particularly, six specimens were cast for each mixture by mechanically mixing the cement powder with the nano-modified suspensions for several minutes (Figure 1d,e). The resulting pastes were poured into oiled molds and vibrated until the frequency of emerging air bubbles decreased significantly (Figure 1f,g). For each mixture, four square copper meshes were put into three of the six samples to serve as electrodes for measuring the electrical resistivity after the curing period (Figure 1h). The position and geometry of the copper meshes are represented in Figure 2.

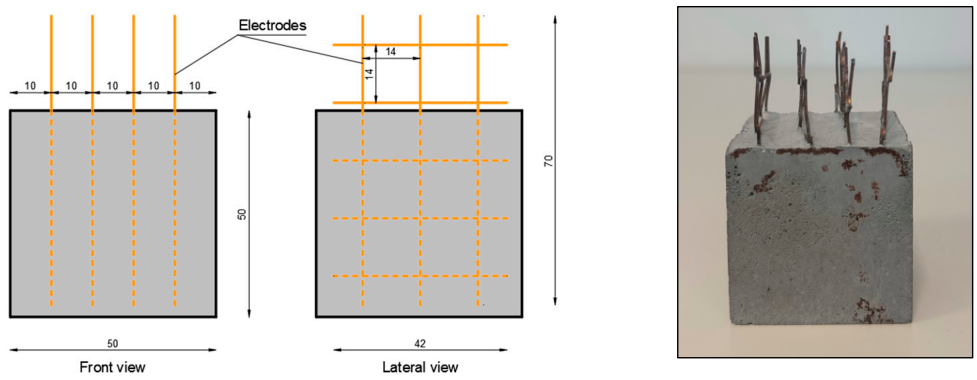


Figure 2. (**a**) Geometry of specimens and electrodes (dimensions are in mm). (**b**) Sample after the curing period.

Subsequently, all samples were covered with plastic sheets and kept at a temperature of 20 °C (±2 °C) and a relative humidity of approximately 65%. After 24 h, the samples were removed from the molds, weighed, and then fully immersed in a tank of distilled water at 20 °C (±2 °C) for 27 days. On the 27th day, the samples were removed from water and dried at 70 °C (±2 °C) and 10% relative humidity for approximately 72 h.

To verify the reduction of water content in the samples, weight measurements were taken every 24 h until the difference between two successive weighings was negligible. These curing and drying steps were conducted to minimize the effect of free water on the sensors, which could adversely affect their effective electrical resistance.

2.4. Electrical Measurements

Although more complex and time-consuming, the four-probe method was chosen in this study to evaluate the electrical resistance of the samples after the curing period. To ensure the best accuracy in resistance measurement, tests were performed using a digital multimeter (DMM7510 7.5 Digit Graphical Sampling Multimeter, Keithley Instrument, Tektronix Inc., Beaverton, OR, USA). As shown in Figure 3a, one set of test cables—INPUT HI, INPUT LO—was connected to the outermost electrodes, positioned 3 cm apart, while a second set of cables—SENSE HI, SENSE LO—was connected to the innermost electrodes, placed 1 cm apart. The multimeter was connected to a computer via LAN cable, and a Python 3.13 script was used for data acquisition (Figure 3a).

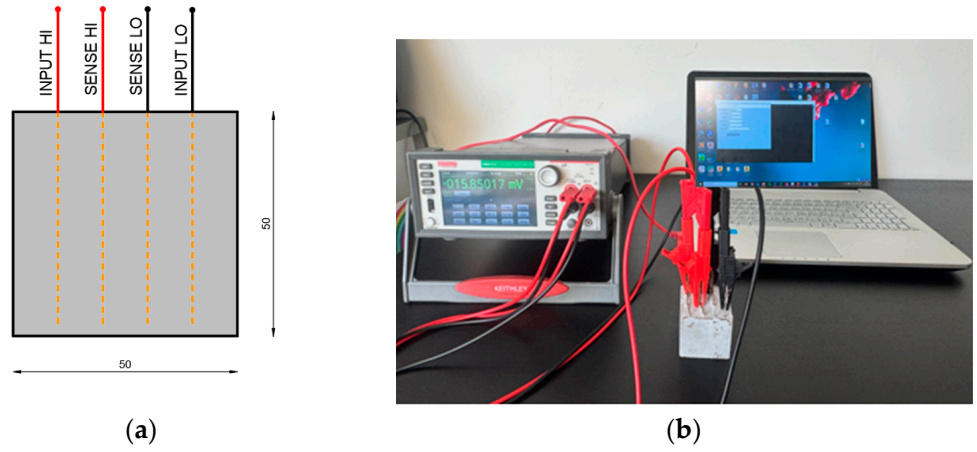


Figure 3. (**a**) Connection of test cables to sample electrodes (dimensions are in mm). (**b**) Test setup for electric resistance acquisition.

For each sample, 10 electrical resistance measurements were made per second, with the experimental procedure lasting 10 s. Using the mean value of electrical resistance measurements (R_{avg}), the electrical resistivity (ρ) and electrical conductivity of the material (σ) were calculated as follows:

$$\rho = R_{avg}\frac{A}{L} \quad (1)$$

$$\sigma = \frac{1}{\rho} \quad (2)$$

where A is the cross-section of the cement-based sensor and L is the distance between the inner electrodes.

2.5. Experimental Results

The influence of MWCNTs content on electrical measurements is presented in Figure 4, where each data point represents the average results of ρ and σ obtained from the three samples of each mixture. As also highlighted by the review of the available literature on cementitious or polymer composites containing different conductive charges [36,37], the curve appears with a typical "S" shape, indicative of the percolation phenomenon, i.e., the transformation of a material from an insulating to a conductive one, that occurs when a critical concentration of conductive charges is reached, allowing the formation of continuous conductive networks and a sudden increase in conductivity.

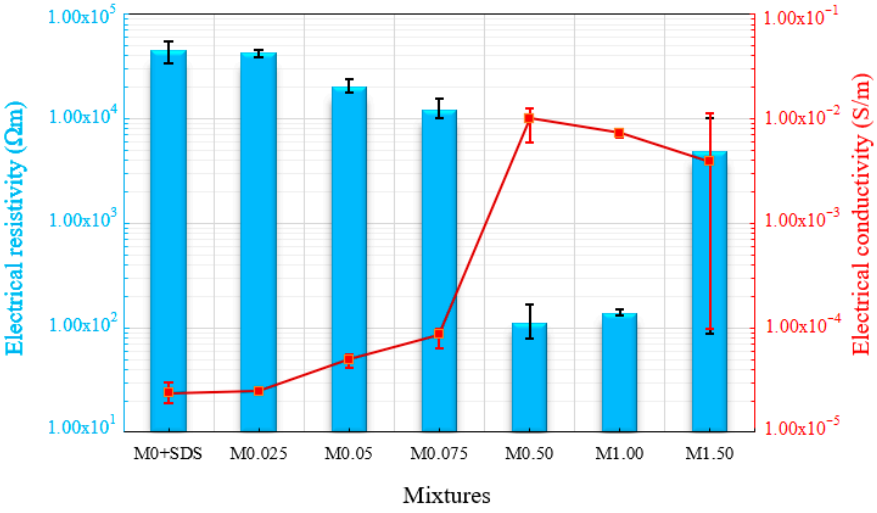


Figure 4. Logarithmic plot of the electrical resistivity and conductivity of mixtures.

According to our results, it is evident that the control mixture (M0) exhibits the lowest value of electrical conductivity and then starts to rise with increasing MWCNT content. In particular, while the addition of 0.025 wt% of MWCNTs produced no change in electrical conductivity, a drastic increase was recorded when 0.5 wt% was added, with the conductivity becoming more than 400 times that of the M0 mixture. Further increases in nanofiller content do not lead to a substantial change in conductivity. Within the investigated MWCTN contents, it can be concluded that the percolation zone is identified between 0.05 and 0.5 wt%. It is interesting to note that the percolation zone obtained in this experimental activity is notably lower than those reported in previous investigations [31,38–45]. This discrepancy is attributed not only to the content of filler embedded in the composite but also to their aspect ratio. An elevated aspect ratio increases the probability of contact and overlap between individual MWCNTs. This characteristic effectively reduces the percolation threshold, which represents the minimum concentration of conductive filler required to establish a continuous conductive pathway. Another contributing factor may

be the use of SDS for the dispersion of MWCNTs in water. As discussed in [42,43], SDS can promote the formation of micelles that trap air, leading to foam generation and, consequently, increased porosity in the cement matrix. This phenomenon results in a reduction in the overall density of the material and an increase in internal porosity, both of which may influence the percolation behavior and the measured electrical conductivity.

3. Analytical Investigation

3.1. A Brief Outline of the Micromechanical Model

In order to predict the experimentally measured electrical conductivity of cement-based composites, a micromechanical model developed by the same authors of the present paper [32] is here employed, without accounting for the contributions of electron hopping as well as the effects of agglomeration and segregation of MWCNTs.

The theoretical foundations of the proposed model are rooted in those originally developed by Deng and Zheng [25] and further extended by Takeda et al. [26] for CNT-based polymer composites, which have been adapted to account for the specific characteristics of cementitious matrices. The model accounts for the effects of CNT volume fraction (ν^N), percolation threshold (ν_C^N), aspect ratio (A_r), conductivity anisotropy, CNT non-straightness, and the quantum tunneling effect between adjacent nanotubes.

In the model, nanotubes are simplified as solid cylinders, and two primary types of conductive networks are considered: Type I—direct overlapping contacts, and Type II—tunneling-dominated contacts, without physical overlap. Each effective nanotube—comprising the CNT of length l^N and diameter d^N and its surrounding inter-matrix region with thickness t_i^{IM}—is treated as a single nanoscale filler.

Based on these assumptions, the expressions of the electrical conductivity for CNT-based composites, σ_i^C, featuring Type I and Type II conductive networks, are obtained as follows:

$$\frac{\sigma_i^C}{\sigma^M} = \begin{cases} 1 + \xi \frac{\nu^N}{3\lambda^2} \frac{1}{\sigma^M} \frac{4l^N}{\frac{4l^N}{\sigma^N} + \frac{\pi\, h^2 t_I^{IM}}{e^2 (2m\varphi)^{1/2}} exp\left(\frac{4\pi t_I^{IM}}{h}(2m\varphi)^{1/2}\right)}, & (i = I) \\ 1 + \xi \frac{\nu^N}{3\lambda^2} \frac{1}{\sigma^M} \frac{l^N}{\frac{l^N}{\sigma^N} + \frac{h^2 t_{II}^{IM}}{e^2 (2m\varphi)^{1/2}} exp\left(\frac{4\pi t_{II}^{IM}}{h}(2m\varphi)^{1/2}\right)}, & (i = II) \end{cases} \tag{3}$$

where e, h, and m are the unit electric charge, the Planck's constant, and the mass of an electron, respectively. The parameter $\varphi = \eta(eV)$ is the potential barrier height, which represents the energy acquired by an electron as it moves across a potential difference of one volt, where η is scalar. Moreover, σ^M and σ^N are the electrical conductivity of the matrix material and the longitudinal electrical conductivity of the carbon nanotube, respectively.

The parameter ξ quantifies the fraction of percolated nanotubes and is defined as follows [25,28]:

$$\xi = \begin{cases} 0 & 0 \le \nu^N < \nu_C^N \\ \dfrac{(\nu^N)^{\frac{1}{3}} - (\nu_C^N)^{\frac{1}{3}}}{1 - (\nu_C^N)^{\frac{1}{3}}} & \nu_C^N \le \nu^N \le 1 \end{cases} \tag{4}$$

where ν_C^N represents the percolation threshold, which—assuming a uniform random CNTs distribution—can be estimated as follows [28]:

$$\nu_C^N(H) = \frac{9H(1-H)}{2 + 15H - 9H^2} \tag{5}$$

being

$$H = \frac{1}{A_r^2 - 1}\left[\frac{A_r}{\sqrt{A_r^2 - 1}} ln\left(A_r + \sqrt{A_r^2 - 1}\right) - 1\right] \quad (6)$$

The waviness ratio, λ, defined as the ratio between the nanotube length, l^N, and the minimum distance between the two ends of the wavy CNT, $\bar{l}^E$, is used to model them as equivalent straight nanotubes.

The novelty of the model lies in the adoption of a new approach, based on well-established quantum mechanical principles, to account for the tunneling effect in estimating the thickness of the inter-nanotube matrix region, t_i^{IM}, which is defined for both configurations as follows [32]:

$$t_i^{IM} = \frac{1}{2\sqrt{\eta}}\left(v^N\right)^{\beta} \quad in\ [nm], \quad (i = I, II) \quad (7)$$

where β is a constant calibrated using experimental data from the literature [31,38,44,45]. The value depends on the type of cementitious material, with typical values found to be approximately -0.10 for cement pastes, -0.12 for mortars, and -0.14 for concretes.

3.2. Analytical Predictions and Comparison with Experimental Results

The analytical predictions of the electrical conductivity of cement pastes were compared with the experimental results across different MWCNT volume fractions, v^N. The analysis accounted for both conductive mechanisms (Type I and Type II), exploring different intrinsic conductivities of the MWCNTs, σ^N, ranging from 10 S/m to 10^5 S/m [30,31], as well as their length, l^N, which was specifically set to 10 µm, 20 µm, and 30 µm. Moreover, a waviness ratio, λ, of 1.50 was considered, while the matrix electrical conductivity, σ^M, was fixed at 2.37×10^{-5} S/m. Finally, the influence of the surfactant—forming a partially insulating layer on the surface of the nanotubes, which significantly impairs the electrical properties of the material—was simulated in the micromechanical model by increasing the potential barrier height, using values of η equal to 1.5 and 3, as suggested in [31].

As observed in Figure 5a–f, the analytical results are in good agreement with the experimental findings, highlighting a sharp increase in conductivity with increasing v^N, especially beyond the percolation threshold. Furthermore, with η held constant, longer nanotubes yield greater predicted conductivity, particularly at lower volume fractions, as a consequence of improved percolation and network connectivity. The theoretical outcomes align well with the experimental data when σ^N falls within the range of 10 S/m to 100 S/m. Notably, these values are consistent with the intrinsic conductivity of the MWCNTs employed, reinforcing the agreement between analytical predictions and experimental results.

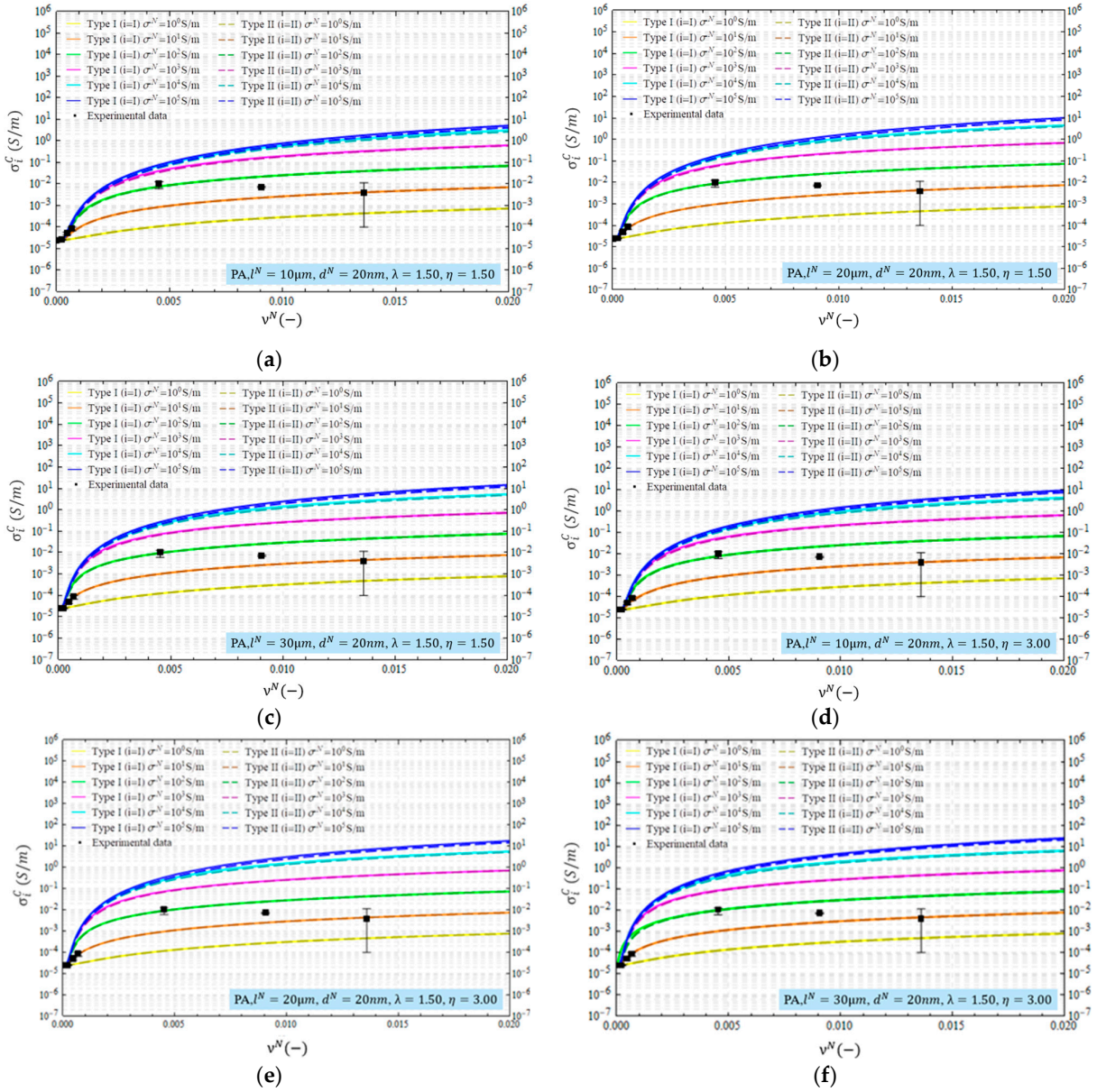


Figure 5. Comparison between micromechanical model predictions and experimental results of electrical conductivity of MWCNTs cement–matrix composites for different geometry parameter and η values: (**a**) l^N = 10 μm, d^N = 20 nm, λ = 1.50, η = 1.50; (**b**) l^N = 20 μm, d^N = 20 nm, λ = 1.50, η = 1.50; (**c**) l^N = 30 μm, d^N = 20 nm, λ = 1.50, η = 1.50; (**d**) l^N = 10 μm, d^N = 20 nm, λ = 1.50, η = 3.00; (**e**) l^N = 20 μm, d^N = 20 nm, λ = 1.50, η = 3.00; (**f**) l^N = 30 μm, d^N = 20 nm, λ = 1.50, η = 3.00.

4. Conclusions

This work combined experimental characterization and analytical modeling to investigate the electrical behavior of cementitious composites reinforced with Multi-Walled Carbon Nanotubes (MWCNTs). Specimens with different MWCNT contents were produced using a controlled dispersion protocol to ensure uniform nanofiller distribution, and their electrical properties were thoroughly assessed. Due to the use of SDS and MWCNTs with a high aspect ratio, the experimental results show a clear percolation zone between 0.05 wt% and 0.5 wt%. Subsequently, to capture the electrical conductivity behavior of the prepared CNT-based cementitious composites, a simple micromechanical model, incorporating nanotube geometry, waviness, concentration, and quantum tunneling effects, was employed. The correlation between model predictions and measured data confirms the

model's capability to accurately describe how the internal characteristics of CNT-based cement composites influence their electrical behavior. These findings provide a valuable foundation for designing advanced multifunctional composites for real-time Structural Health Monitoring applications.

Author Contributions: Conceptualization, R.P., A.L., G.L. (Gerarda Landi), G.L. (Giuseppe Lovisi), and L.F.; methodology, R.P., A.L., G.L. (Gerarda Landi), and G.L. (Giuseppe Lovisi); software, R.P., A.L., G.L. (Gerarda Landi), and G.L. (Giuseppe Lovisi); validation, R.P., A.L., G.L. (Gerarda Landi), G.L. (Giuseppe Lovisi), and L.F.; formal analysis, R.P., A.L., G.L. (Gerarda Landi), and G.L. (Giuseppe Lovisi); investigation, R.P., A.L., G.L. (Gerarda Landi), and G.L. (Giuseppe Lovisi); resources, R.P., A.L., G.L. (Gerarda Landi), and G.L. (Giuseppe Lovisi); data curation, R.P., A.L., G.L. (Gerarda Landi), and G.L. (Giuseppe Lovisi); writing—original draft preparation, R.P., A.L., G.L. (Gerarda Landi), and G.L. (Giuseppe Lovisi); writing—review and editing, R.P., A.L., G.L. (Gerarda Landi), G.L. (Giuseppe Lovisi), and L.F.; visualization, R.P. and L.F.; supervision, R.P. and L.F.; project administration, R.P. and L.F.; funding acquisition, R.P. and L.F. All authors have read and agreed to the published version of the manuscript.

Funding: The authors gratefully acknowledge the financial support of the Italian Ministry of University and Research (MUR): Research Grant PRIN 2020 No. 2020EBLPLS on "Opportunities and challenges of nanotechnology in advanced and green construction materials", by the National Recovery and Resilience Plan (NRRP), Mission 4, Component 2, Investment 1.1, Call for tender No. 104 published on 2 February 2022 by the Italian Ministry of University and Research (MUR), funded by the European Union—NextGenerationEU—Project Titles 'Intelligent Systems for Infrastructural Diagnosis in smart-concretE (ISIDE)'—grant number: 2022S88WAY—CUP D53D23008820006.

Institutional Review Board Statement: Not applicable.

Informed Consent Statement: Informed consent was obtained from all subjects involved in the study.

Data Availability Statement: Data will be made available upon request.

Conflicts of Interest: The authors declare no conflict of interest.

References

1. Hassani, S.; Mousavi, M.; Gandomi, A.H. Structural Health Monitoring in Composite Structures: A Comprehensive Review. *Sensors* **2022**, *22*, 153. [CrossRef]
2. Aktan, E.; Bartoli, I.; Glišić, B.; Rainieri, C. Lessons from Bridge Structural Health Monitoring (SHM) and Their Implications for the Development of Cyber-Physical Systems. *Infrastructures* **2024**, *9*, 30. [CrossRef]
3. Lee, S.-J.; You, I.; Zi, G.; Yoo, D.-Y. Experimental Investigation of the Piezoresistive Properties of Cement Composites with Hybrid Carbon Fibers and Nanotubes. *Sensors* **2017**, *17*, 2516. [CrossRef] [PubMed]
4. Ghahremani, B.; Enshaeian, A.; Rizzo, P. Bridge Health Monitoring Using Strain Data and High-Fidelity Finite Element Analysis. *Sensors* **2022**, *22*, 5172. [CrossRef] [PubMed]
5. Barrias, A.; Casas, J.R.; Villalba, S. A Review of Distributed Optical Fiber Sensors for Civil Engineering Applications. *Sensors* **2016**, *16*, 748. [CrossRef]
6. Mardanshahi, A.; Sreekumar, A.; Yang, X.; Barman, S.K.; Chronopoulos, D. Sensing Techniques for Structural Health Monitoring: A State-of-the-Art Review on Performance Criteria and New-Generation Technologies. *Sensors* **2025**, *25*, 1424. [CrossRef]
7. Taheri, S. A Review on Five Key Sensors for Monitoring of Concrete Structures. *Constr. Build. Mater.* **2019**, *204*, 492–509. [CrossRef]
8. Rizzo, P.; Enshaeian, A. Challenges in Bridge Health Monitoring: A Review. *Sensors* **2021**, *21*, 4336. [CrossRef]
9. Ferreira, A.D.B.; Nóvoa, P.R.; Marques, A.T. Multifunctional Material Systems: A State-of-the-Art Review. *Compos. Struct.* **2016**, *151*, 3–35. [CrossRef]
10. Ha, G.-J.; Cho, C.-G.; Kang, H.-W.; Feo, L. Seismic Improvement of RC Beam–Column Joints Using Hexagonal CFRP Bars Combined with CFRP Sheets. *Compos. Struct.* **2013**, *95*, 464–470. [CrossRef]
11. Kim, Y.Y.; Lee, B.Y.; Bang, J.-W.; Han, B.-C.; Feo, L.; Cho, C.-G. Flexural Performance of Reinforced Concrete Beams Strengthened with Strain-Hardening Cementitious Composite and High Strength Reinforcing Steel Bar. *Compos. Part B Eng.* **2014**, *56*, 512–519. [CrossRef]
12. Feo, L.; Ascione, F.; Penna, R.; Lau, D.; Lamberti, M. An Experimental Investigation on Freezing and Thawing Durability of High-Performance Fiber Reinforced Concrete (HPFRC). *Compos. Struct.* **2020**, *234*, 111673. [CrossRef]

13. Martinelli, E.; Pepe, M.; Penna, R.; Feo, L. A Cracked-Hinge Approach to Modelling High Performance Fiber-Reinforced Concrete. *Compos. Struct.* **2021**, *273*, 114277. [CrossRef]
14. Penna, R.; Feo, L.; Martinelli, E.; Pepe, M. Theoretical Modelling of the Degradation Processes Induced by Freeze–Thaw Cycles on Bond-Slip Laws of Fibres in High-Performance Fibre-Reinforced Concrete. *Materials* **2022**, *15*, 6122. [CrossRef] [PubMed]
15. Feo, L.; Lambiase, A.; Martinelli, E.; Penna, R.; Pepe, M. On the Effect of Carbon Nanotubes in Ultra-High Performance Fiber Reinforced Concrete. *Procedia Struct. Integr.* **2023**, *47*, 800–811. [CrossRef]
16. Tian, Z.; Li, Y.; Zheng, J.; Wang, S. A State-of-the-Art on Self-Sensing Concrete: Materials, Fabrication and Properties. *Compos. Part B Eng.* **2019**, *177*, 107437. [CrossRef]
17. Chung, D.D.L. Self-Sensing Concrete: From Resistance-Based Sensing to Capacitance-Based Sensing. *Int. J. Smart Nano Mater.* **2020**, *11*, 1–19. [CrossRef]
18. Han, B.G.; Wang, Y.Y.; Dong, S.F.; Zhang, L.; Ding, S.; Yu, X.; Ou, J. Smart Concretes and Structures: A Review. *J. Intell. Mater. Syst. Struct.* **2015**, *26*, 1303–1345. [CrossRef]
19. Wang, Y.; Zhang, L. Development of Self-Sensing Cementitious Composite Incorporating Hybrid Graphene Nanoplates and Carbon Nanotubes for Structural Health Monitoring. *Sens. Actuators A Phys.* **2022**, *336*, 113367. [CrossRef]
20. Yu, X.; Kwon, E. A Carbon Nanotube/Cement Composite with Piezoresistive Properties. *Smart Mater. Struct.* **2009**, *18*, 055010. [CrossRef]
21. Han, B.; Ding, S.; Yu, X. Intrinsic Self-Sensing Concrete and Structures: A Review. *Measurement* **2015**, *59*, 110–128. [CrossRef]
22. An, S.H.; Kim, K.Y.; Lee, J.U. Reinforcement of Cement Nanocomposites through Optimization of Mixing Ratio between Carbon Nanotube and Polymer Dispersing Agent. *Polymers* **2024**, *16*, 428. [CrossRef]
23. de Almeida Carísio, P.; dos Santos Mendonça, Y.G.; Soares, C.F.T.; Reales, O.A.M.; de Moraes Rego Fairbairn, E.; Filho, R.D.T. Dispersion of Carbon Nanotubes with Different Types of Superplasticizer as a Dispersing Agent for Self-Sensing Cementitious Materials. *Appl. Sci.* **2021**, *11*, 8452. [CrossRef]
24. Konsta-Gdoutos, M.S.; Metaxa, Z.S.; Shah, S.P. Highly Dispersed Carbon Nanotube Reinforced Cement Based Materials. *Cem. Concr. Res.* **2010**, *40*, 1052–1059. [CrossRef]
25. Deng, F.; Zheng, Q.S. An Analytical Model of Effective Electrical Conductivity of Carbon Nanotube Composites. *Appl. Phys. Lett.* **2008**, *92*, 071902. [CrossRef]
26. Takeda, T.; Shindo, Y.; Kuronuma, Y.; Narita, F. Modeling and Characterization of the Electrical Conductivity of Carbon Nanotube-Based Polymer Composites. *Polymer* **2011**, *52*, 3852–3856. [CrossRef]
27. Seidel, G.D.; Lagoudas, D.C. A Micromechanics Model for the Electrical Conductivity of Nanotube–Polymer Nanocomposites. *J. Compos. Mater.* **2009**, *43*, 917–941. [CrossRef]
28. Feng, C.; Jiang, L. Micromechanics Modeling of the Electrical Conductivity of Carbon Nanotube–Polymer Nanocomposites. *Compos. Part A Appl. Sci. Manuf.* **2013**, *47*, 143–149. [CrossRef]
29. Alamusi; Hu, N. Numerical Simulations on Piezoresistivity of CNT/Polymer Based Nanocomposites. *Comput. Mater. Contin.* **2010**, *20*, 101–118.
30. García-Macías, E.; D'Alessandro, A.; Castro-Triguero, R.; Pérez-Mira, D.; Ubertini, F. Micromechanics Modeling of the Uniaxial Strain-Sensing Property of Carbon Nanotube Cement-Matrix Composites for SHM Applications. *Compos. Struct.* **2017**, *163*, 195–215. [CrossRef]
31. García-Macías, E.; D'Alessandro, A.; Castro-Triguero, R.; Pérez-Mira, D.; Ubertini, F. Micromechanics Modeling of the Electrical Conductivity of Carbon Nanotube Cement-Matrix Composites. *Compos. Part B Eng.* **2017**, *108*, 451–469. [CrossRef]
32. Penna, R.; Landi, G.; Lovisi, G.; Lambiase, A.; Feo, L. Micromechanical Modeling of the Piezoelectric Behavior of CNT Cement-Matrix Composites. *Compos. Part B Eng.* **2025**, *306*, 112810. [CrossRef]
33. Heidelberg Materials. Available online: https://www.heidelbergmaterials.it (accessed on 23 June 2025).
34. Sodium Laurylsulfate, Carlo Erba Reagents. CAS No. 151-21-3. Available online: https://www.carloerbareagents.com (accessed on 23 June 2025).
35. AsItaly Advanced Scientific. Available online: https://www.asitaly.it (accessed on 23 June 2025).
36. Xie, P.; Gu, P.; Beaudoin, J.J. Electrical Percolation Phenomena in Cement Composites Containing Conductive Fibres. *J. Mater. Sci.* **1996**, *31*, 4093–4097. [CrossRef]
37. Kim, Y.J.; Shin, T.S.; Choi, H.D.; Kwon, J.H.; Chung, Y.C.; Yoon, H.G. Electrical Conductivity of Chemically Modified Multiwalled Carbon Nanotube/Epoxy Composites. *Carbon* **2005**, *43*, 23–37. [CrossRef]
38. D'Alessandro, A.; Ubertini, F.; Materazzi, A.L. Self-Sensing Concrete Nanocomposites for Smart Structures. *Int. J. Archit. Civ. Constr. Sci.* **2016**, *10*, 599–604.
39. Naeem, F.; Lee, H.K.; Kim, H.K.; Nam, I.W. Flexural Stress and Crack Sensing Capabilities of MWNT/Cement Composites. *Compos. Struct.* **2017**, *175*, 86–100. [CrossRef]
40. Jiang, S.; Zhou, D.; Zhang, L.; Ouyang, J.; Yu, X.; Cui, X.; Han, B. Comparison of Compressive Strength and Electrical Resistivity of Cementitious Composites with Different Nano- and Micro-Fillers. *Arch. Civ. Mech. Eng.* **2018**, *18*, 60–68. [CrossRef]

41. del Moral, B.; Baeza, F.J.; Navarro, R.; Galao, O.; Zornoza, E.; Vera, J.; Farcas, C.; Garcés, P. Temperature and Humidity Influence on the Strain Sensing Performance of Hybrid Carbon Nanotubes and Graphite Cement Composites. *Constr. Build. Mater.* **2021**, *284*, 122786. [CrossRef]
42. Sobolkina, A.; Mechtcherine, V.; Khavrus, V.; Maier, D.; Mende, M.; Ritschel, M.; Leonhardt, A. Dispersion of Carbon Nanotubes and Its Influence on the Mechanical Properties of the Cement Matrix. *Cem. Concr. Compos.* **2012**, *34*, 1104–1113. [CrossRef]
43. Szeląg, M. Mechano-Physical Properties and Microstructure of Carbon Nanotube Reinforced Cement Paste after Thermal Load. *Nanomaterials* **2017**, *7*, 267. [CrossRef]
44. Xing, G.; Xu, Y.; Zhao, Z.; Chen, S. Piezoresistive Properties of Well-Dispersed Carbon Nanotubes (CNTs) Modified Cement Paste. *J. Build. Eng.* **2024**, *95*, 110364. [CrossRef]
45. Meoni, A.; D'Alessandro, A.; Downey, A.; García-Macías, E.; Rallini, M.; Materazzi, A.L.; Torre, L.; Laflamme, S.; Castro-Triguero, R.; Ubertini, F. An Experimental Study on Static and Dynamic Strain Sensitivity of Embeddable Smart Concrete Sensors Doped with Carbon Nanotubes for SHM of Large Structures. *Sensors* **2018**, *18*, 831. [CrossRef]

Disclaimer/Publisher's Note: The statements, opinions and data contained in all publications are solely those of the individual author(s) and contributor(s) and not of MDPI and/or the editor(s). MDPI and/or the editor(s) disclaim responsibility for any injury to people or property resulting from any ideas, methods, instructions or products referred to in the content.